Microgravity Science and Technology (2023) 35:39
https://doi.org/10.1007/s12217-023-10060-1

RESEARCH

Beijing Drop Tower Microgravity Adjustment Towards $10^{-3} \sim 10^{-5}$g Level by Cold-Gas Thrusters

Chu Zhang[1] · Chao Yang[1] · Liang Hu[1] · Shuyang Chen[1,2] · Yifan Zhao[1] · Li Duan[1,2] · Qi Kang[1,2]

Received: 27 December 2022 / Accepted: 14 June 2023 / Published online: 25 July 2023

Abstract

Drop tower is an important facility for conducting microgravity experiments on the ground. Since the Beijing drop tower was put into operation in 2003, a large number of scientific experiments have been carried out in the fields of microgravity fluid physics, combustion, materials science and fundamental physics. The drop tower has two operation modes: single capsule falling and double capsule falling, with the microgravity levels reaching 10^{-2}g ~ 10^{-3}g and 10^{-5}g respectively. In order to meet the demand of multi-level microgravity levels in ground microgravity experiments, a double capsule microgravity level control system based on the cold-gas micro thruster is developed. The micro thrusters are mounted in the inner capsule of the double capsule system. During the fall of the double capsule, the cold-gas micro thrusters thrust in the opposite direction of the movement of the structure, which increases the resistance of the inner capsule to realize the control of microgravity level. The measurement results of the high-precision accelerometer show that the $10^{-3} \sim 10^{-5}$g microgravity level can be controlled by this system.

Keywords Drop Tower · Microgravity · Cold-gas thruster · Accelerometer

Introduction

In the twenty-first century, China has made great progress in manned spaceflight (Yidong et al. 2016), space station construction (Gu 2021), outer space development and utilization (Zhou et al. 2022), deep space exploration (Peng et al. 2020) and other fields. Microgravity science and application is an important part of these fields. With the gradual construction of China's space station in orbit and the rapid development of space exploration, the development of microgravity science is becoming more and more active, and many important achievements have been made.

On the ground or in space, there are a variety of experimental platforms for microgravity experiments, as shown in Table 1.

Compared with other facilities, although the microgravity time of drop tower is relatively short, it has the obvious advantages of high microgravity level, relatively low cost, more experimental opportunities, higher frequency of use, the ability to use precision measuring instruments, and the convenience of human intervention. Therefore, drop tower has become the main facility for microgravity scientific experiments.

In 1966, NASA put into operation the drop shaft of the then NASA Lewis Research Center in Cleveland. Initially,

Chu Zhang and Chao Yang are co-first authors.

✉ Liang Hu
hl@imech.ac.cn

✉ Qi Kang
kq@imech.ac.cn

Chu Zhang
zhangchu@imech.ac.cn

Chao Yang
yangchao1@imech.ac.cn

Shuyang Chen
chenshuyang@imech.ac.cn

Yifan Zhao
zyf999913@163.com

Li Duan
duanli@imech.ac.cn

[1] National Micro Gravity Laboratory, Institute of Mechanics, CAS, Beijing 100190, People's Republic of China

[2] School of Engineering Science, University of Chinese Academy of Sciences, Beijing 100190, People's Republic of China

Table 1 Characteristics of different microgravity experimental platforms

No.	Microgravity experimental platform	Microgravity level	Microgravity time	Experimental convenience
1	Manned spacecraft/space station	~10^{-3}g	long-term	Long launch cycle, many restrictions
2	recoverable satellite	10^{-3}~10^{-5}g	long-term	Long launch cycle, many restrictions
3	Drag-free satellite	10^{-8}~10^{-12}g	long-term	Long launch cycle, many restrictions
4	Microgravity sounding rocket	~10^{-5}g	5~16min	Special facilities, short launch cycle
5	Drop tower/well	10^{-3}~10^{-5}g	2~10s	experiments many times a day
6	Free fall of balloon	10^{-2}~10^{-4}g	30~40s	Once a week
7	Weightless aircraft	10^{-2}~10^{-3}g	15~40s	experiments many times a day

it was not intended for general scientific purposes, but only to study the behavior of kerosene and cryogenic propellants during ballistic phases of a rocket flight. Its purpose was therefore to support Gemini, Mercury, and Saturn rocket development. The precursor for this was initially a small 2.2s drop facility also at now NASA Glenn Research Center in Cleveland, which is still used intensively today in parallel with the large drop shaft (NASA 2017). Germany built a drop tower in Bremen in the early 1990s. It had a height of 146m and offered a 4.7s microgravity time, with the microgravity level of 10^{-5}~10^{-6}g. In 2004, the tower was installed with an ejection system, which doubled the microgravity time (Selig et al. 2010). Soon after the Bremen drop tower was put into operation, Japan established two microgravity wells with depths of 710m and 150m, providing microgravity times of 10s and 4.5s respectively (Koide 2001). They are now closed. India IIT Madras has built a drop tower with a free fall height of 30.5m, a microgravity time of 2.5 s, and a microgravity level of 10^{-4}g (Nikhil et al. 2018). The University of Queensland in Australia has built a drop tower with a microgravity time of 2s and a microgravity level of 10^{-4}~10^{-6}g (Steinberg 2008). Tsinghua University Free Fall Facility (TUFF) has a free fall time of 2.2s and a microgravity level of 10^{-3}g (Luo et al. 2021). The electromagnetic launching microgravity experimental facility of Space Application Center of Chinese Academy of Sciences has a microgravity time of 4s and a microgravity level of 10^{-5}g (Zhang et al. 2021).

Beijing drop Tower was built by the Institute of Mechanics of Chinese Academy of Sciences and operated by the microgravity laboratory. The microgravity time is 3.6 s, the single capsule microgravity level is 10^{-3}~10^{-2}g, the double capsule microgravity level is 10^{-5}g, and the deceleration overload is about 20g. The drop tower facility is composed of experimental capsule components, deceleration recovery system, release system, control system, measurement system and auxiliary facilities (Xiaoqian et al. 2005).

See Fig. 1 for the structure of double capsule. The outer capsule has a diameter of 1010 mm and a total length of about 3m. It is a light, thin-walled, compression composite aluminum alloy shell structure. The outer capsule falls in the atmospheric environment. Its axisymmetric bullet shape is to reduce the aerodynamic resistance acting on the capsule when falling. The inner capsule is a thin-walled cylindrical structure with a diameter of 700 mm and a height of 1000 mm. During the experiment, there is a vacuum between the outer capsule and the inner capsule. The outer capsule can be used for the free fall test separately, and the test load can be installed inside the outer capsule. When the experiment requires a high microgravity level, the double capsule working mode is adopted, and the experimental device is installed in the inner capsule. During the experiment, the inner capsule falls freely in the vacuum environment inside the outer capsule, and the relative speed between the inner and outer capsules is less than 1 m/s. The vacuum environment and the very small relative velocity effectively reduce the aerodynamic resistance acting on the inner capsule when it drops freely, so as to ensure that the experimental device in the inner capsule reaches a microgravity level of 10^{-5}g or even better.

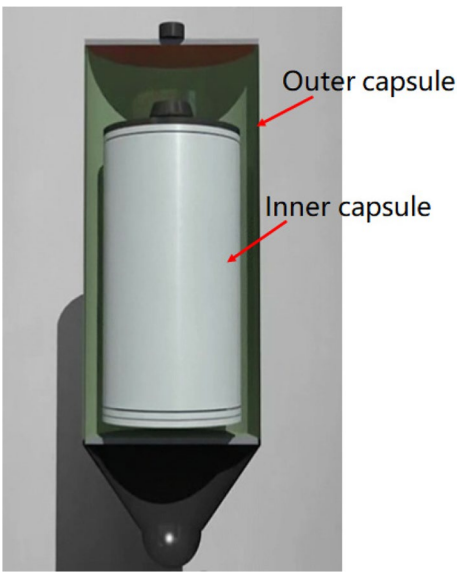

Fig. 1 structure of experiment capsule

The deceleration recovery system of Beijing Drop Tower uses an elastic controllable deceleration recovery device, which includes an electric transducer, a steel wire rope, a recovery net bag that consists of a steel ring, a high-strength woven mesh bag and a high-strength elastic rubber band rope, an industrial computer control unit of the energy consumption resistance box, and an emergency brake cylinder. In the initial state of the experiment, the transducer lifts the net bag to a predetermined height of 22m from the ground (0 m) and keeps it in a hovering standby state, as shown in Fig. 2. The recovery system starts to work 1s before the capsule falls and touches the mesh bag. The mesh bag component starts to slide under its own weight. The transducer has been in a rotating state to reduce the impact on it when the capsule falls and hits the mesh bag. During the whole recovery process, the kinetic energy of the capsule falls and this amount of energy is converted into the kinetic energy of the mesh bag and the elastic potential energy, which are converted into electric energy by the transducer and consumed by the energy consuming resistor. The final speed of the mesh bag and the capsule falling combination is zero, and the elastic rope is in a natural state of tension, thus the whole recovery process is completed. The whole deceleration process is similar to a half sine wave, with an average deceleration overload of ~ 8g and a peak overload of ~ 12g.

This facility adopts electromagnetic release device, as shown in Fig. 3. This mechanism is composed of an electromagnetic suction head assembly, an external capsule suction head assembly, an internal capsule suction head

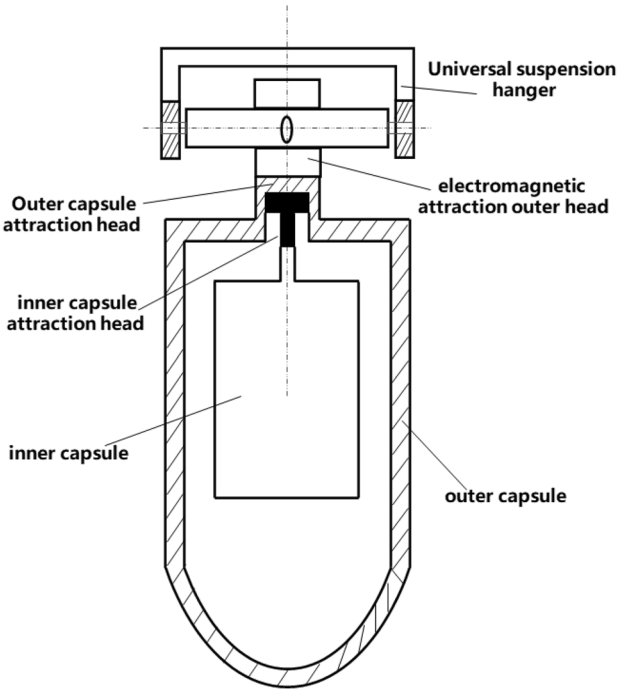

Fig. 3 capsule and release system

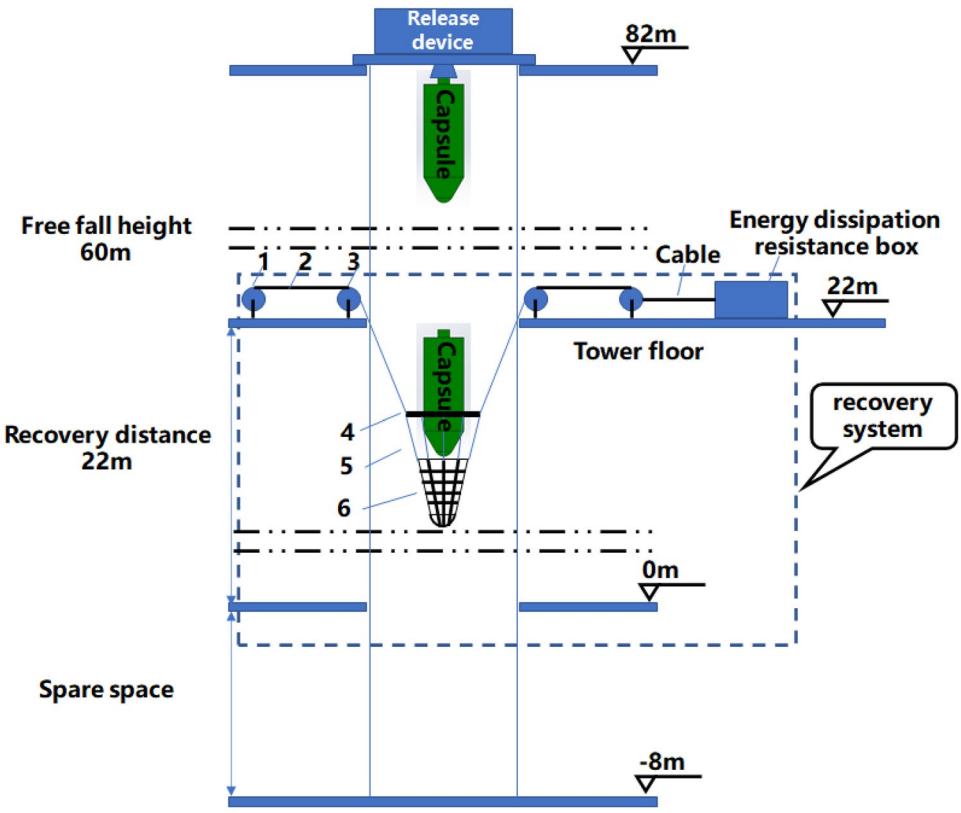

Fig. 2 Deceleration recovery system. 1 transducer, 2 wire ropes, 3 guide wheels, 4 steel rings, 5 high-strength elastic rubber rope set, 6 high-strength woven mesh bag

assembly, an external capsule mechanical locking/unlocking mechanism, an internal capsule mechanical locking/unlocking mechanism, a control system, etc. The release mechanism uses the non-mechanically connected electromagnetic suction and discharge principle. The "force" between the electromagnetic suction head and the suction heads of the outer and inner capsules is connected through the "surface". When the release test capsule assembly starts to fall, it has been separated from the direct contact with the electromagnetic suction head assembly, but the electromagnetic suction head still has suction on the test chamber (inner capsule, outer capsule). The suction gradually decreases with the decrease of the residual magnetic suction of the electromagnetic suction head and the increase of the spacing distance between the test capsule and the electromagnetic suction head, until it completely disappears. The experimental device in the capsule changes from its normal gravity state to microgravity during the experiment, which is not a step mutation process, but a gradual change process. The initial interference of the release process to the experimental device is reduced effectively.

Since its completion in 2003, Beijing drop tower has carried out a wide range of scientific experiments, mainly including research in the fields of microgravity fluid physics, combustion and materials science. For example, capillary flow under microgravity (Wang et al. 2010), suspension drop study (Zhi-Qiang and David 2010), boiling experiment study of distilled water and HFE7500 (Yang et al. 2018), coal combustion mechanism study (Yang et al. 2022), etc. It has made due contributions to promoting the development and progress of space science in China. With the gradual implementation of China's space station project, more and more experimental projects need to carry out matching experiments at the drop tower. Some experiments also put forward new requirements for tower falling. For example, the gravity scaling law (Zhao and Du 2020; Raj et al. 2010) in boiling experiments, the response of surface tension to microgravity levels of different orders (Chen et al. 2021; Hu et al. 2009), and the simulation of microgravity level status of space station fluid tank of different orders.

In order to meet the requirements of ground microgravity experiments for multi-level microgravity levels, a new type of deceleration control system for the inner capsule cold air micro thruster is developed based on the double capsule operation mode. Multiple groups of micro thrusters are installed at the bottom of the inner capsule. They can generate multi-level constant thrust in the opposite direction of falling. Before the release of the double capsule, the output thrust value of the thruster should be set to ensure that the inner capsule is subject to the determined resistance during the free fall process, so as to realize the stable operation of the inner cabin at the low microgravity level. The measurement results of the high-precision accelerometer show that the capsule of the system can achieve 10^{-3}g ~ 10^{-5}g microgravity control.

This paper includes five sections. The first section is the introduction, which briefly introduces the needs and plans of Beijing drop tower and its transformation. The second sections introduces in detail the transformation scheme of Beijing drop tower, the development of the key actuator cold-gas micro thruster, and the calibration of the accelerometer. The third section briefly introduces the construction and experiment process of the drop tower transformation system. The fourth section shows the experimental results and analysis of the inner capsule cold-gas micro thruster deceleration control system. The fifth part is the conclusion of the paper.

Technical Upgrading Scheme for Double Capsule

Technical Upgrading Scheme

According to the technical upgrading requirements of drop tower, the upgrading scheme is designed based on the double capsule mode. In the scheme, cold-gas thrusters are installed at the bottom of the inner capsule to adjust the microgravity level of the inner capsule by adjusting the thrust. A high-precision accelerometer is installed in the inner capsule to measure the real-time acceleration of the inner capsule. As shown in Fig. 4.

In Eqs. (1) and (2), F_{thrust} is the thrust of the cold-gas thruster. The mass of inner capsule is $m = 200$ kg. The accelerometer installed in the inner capsule measures the residual acceleration of the inner capsule, a_{res}.

$$mg - F_{thrust} = ma_{\text{real}} \tag{1}$$

$$F_{thrust} = m(g - a_{\text{real}}) = ma_{\text{res}} \tag{2}$$

when the microgravity level is required to be 10^{-5}g, the cold-gas micro thruster remains closed, and the microgravity level is 10^{-5}g during the falling of the inner capsule. When the capsule acceleration is required to be 10^{-4}g, the output of the cold-gas thrust system is 200mN, and the microgravity level is 10^{-4}g. When the capsule acceleration is required to be 10^{-3}g, the output of the cold-gas thrust system is 2000mN, and the microgravity level is 10^{-3}g.

From the above conditions, we can get the requirements for the cold-gas thruster system as below.

$$min\left(F_{thrust}\right) \geq 200mN \tag{3}$$

$$max\left(F_{thrust}\right) \geq 2000mN \tag{4}$$

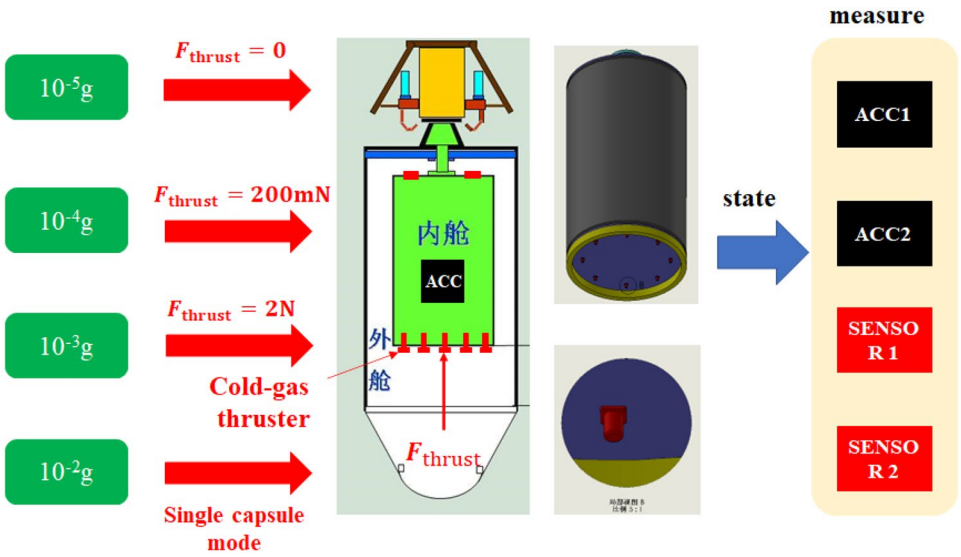

Fig. 4 System scheme

An accelerometer is installed in the inner capsule to measure the residual acceleration of the inner capsule. The accelerometer should have a measurement accuracy of 10^{-5}g and a range of more than 10^{-2}g. The modified capsule system consists of six parts, including the mechanical structure, capsule dropping servo, measurement and control system, high-speed camera, data transmission system, and cold-gas micro propulsion system, as shown in Fig. 5.

Development of Cold-Gas Micro Thruster

According to the thrust requirements of the scheme, the whole cold-gas thrust system includes 24 thrusters. Four of them have a thrust of 50mN and the other 20 have a thrust of 100mN. The 50mN thruster meets the requirements of 10^{-4}g microgravity state. The 100mN force device meets the requirements of 10^{-3}g microgravity state. The tank is filled with high-pressure gas through the filling valve. The pressure sensor 1 of the gas residual channel in the tank judges and decides to open the mechanical stop valve and adjust the mechanical pressure reducing valve to control the air pressure at the front of the thruster. When the solenoid stop valve is powered and activated, the thruster can output the rated thrust. See Fig. 6 for the workflow of the thrust system.

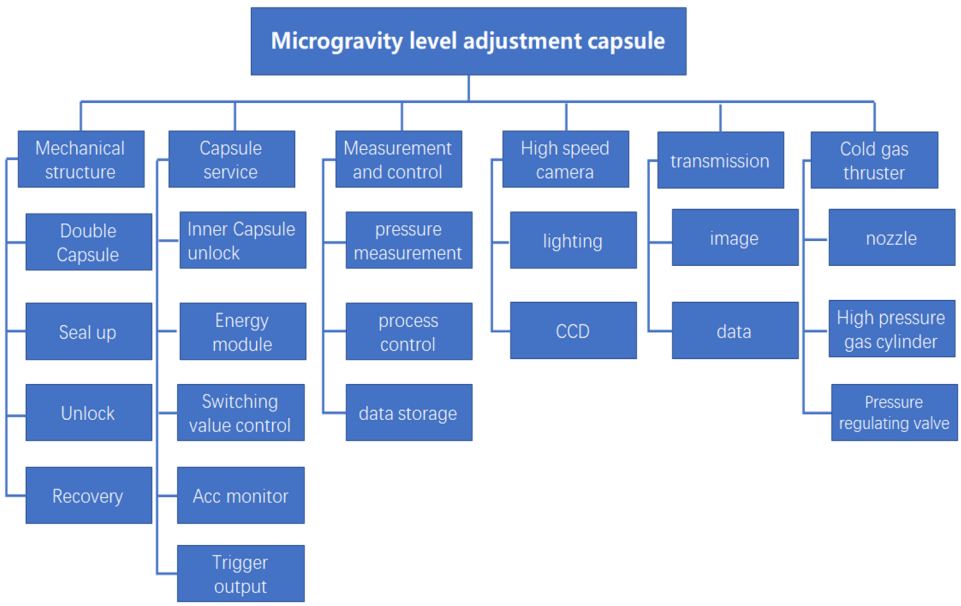

Fig. 5 System structure composition

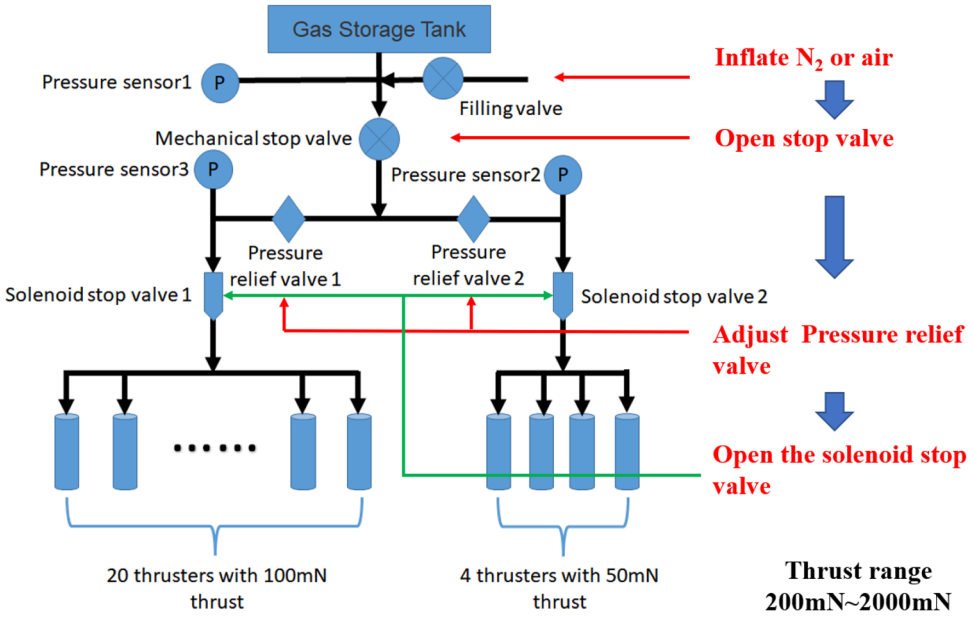

Fig. 6 Cold-gas micro thrust system

Thruster Design

Laval nozzle is the core component of the cold-gas thruster. It can limit the flow of gas and increase the speed of gas injection to reach the predetermined thrust.

The thrust F generated by the nozzle can be expressed as follows:

$$F = \dot{m}v_e + (p_e - p_b)A_e \tag{5}$$

where, $\dot{m}$ is the mass flow of gas, v_e is the velocity of gas at the outlet, p_e is the pressure at the outlet, p_b is the background pressure, A_e is the sectional area of the nozzle outlet.

According to the quasi one-dimensional gas inviscid isentropic flow theory, when the gas in the nozzle flows at a supersonic speed, the expression of the mass flow of gas in the nozzle is as follows:

$$\dot{m} = \sqrt{\gamma}\left(\frac{2}{\gamma+1}\right)^{\frac{\gamma+1}{2(\gamma-1)}}\frac{p_0 A_t}{\sqrt{RT_0}} \tag{6}$$

where, γ is the specific heat ratio of the gas, p_0 is the air pressure at the nozzle inlet, A_t is the throat area of the nozzle, R is the gas constant of a specific gas, T_0 is the gas temperature at the nozzle inlet.

The velocity of gas at the outlet, v_e, can be expressed as:

$$v_e = \sqrt{\frac{2\gamma}{\gamma-1}RT_0\left(1-\frac{T_e}{T_0}\right)} = \sqrt{\frac{2\gamma}{\gamma-1}RT_0\left[1-\left(\frac{p_e}{p_0}\right)^{\frac{\gamma-1}{\gamma}}\right]} \tag{7}$$

where T_e is the gas temperature at the nozzle outlet.

For a shaped nozzle, the air pressure at the nozzle outlet p_e, the area of the nozzle throat A_t, the area of the nozzle outlet A_e, and the air pressure at the nozzle inlet p_0, have the following relationship:

$$\left(\frac{A_e}{A_t}\right)^2 = \frac{\gamma-1}{2\left[\left(\frac{p_0}{p_e}\right)^{\frac{\gamma-1}{\gamma}}-1\right]}\left[\frac{2\left(\frac{p_0}{p_e}\right)^{\frac{\gamma-1}{\gamma}}}{\gamma+1}\right]^{\frac{\gamma+1}{\gamma-1}} \tag{8}$$

where A_e/A_t is called the expansion ratio.

The ideal condition for the gas flow in the nozzle is that the whole nozzle is a continuous flow without shock waves in the nozzle, and the gas pressure at the outlet p_e is equal to the background pressure p_b.

Based on the above theoretical analysis and the thrust demand, if the background pressure and the pressure and temperature at the nozzle inlet are known, the flow rate and the outlet velocity of a specific gas can be calculated according to Eqs. (6) and (7), and the size parameters of the throat and outlet of the nozzle can be determined by substituting them into Eq. (8).

Taking the 100mN thruster nozzle used in this experiment as an example, the initial pressure between the inner and outer capsules is 50 Pa, nitrogen is used as the working medium, the pressure at the inlet is 0.4 MPa, and the ambient temperature is 20℃. Considering the existence of gas viscosity and the three-dimensional velocity divergence, the final design parameters of the nozzle are determined that the nozzle has a throat diameter of 0.5 mm, an outlet diameter of 6.5 mm, and an outlet expansion half-angle of 30 degrees.

The cross-sectional drawing of the thruster head is shown in Fig. 7. The gas channel connector and the nozzle are

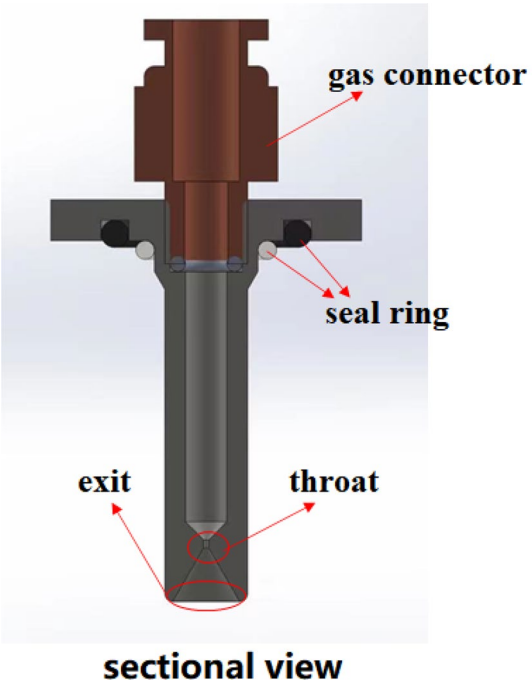

Fig. 7 Cross-section of thruster head

connected by screw threads, with a sealing ring between them. Another sealing ring is added between the nozzle and the mounting surface of the capsule plate.

Thrust Calibration

In order to verify the thrust of the cold-gas micro thruster designed, the thrust of the thruster is tested in a vacuum environment. The layout of the test experiment is shown in Fig. 8. The high-pressure nitrogen reaches the mass flowmeter (Alicat) after being manually adjusted to reduce the pressure. The mass flowmeter can also measure the gas pressure while measuring the flow, and this pressure can be considered as the air pressure at the front of the nozzle. The thruster is installed on the thrust measuring bench that is placed in the vacuum tank. When the thruster works through air injection, it generates torque to drive the test bench to rotate. The torsional deflection displacement is acquisited using the capacitive displacement sensor. Combining the deflection displacement with the torsional coefficient of the elastic element and the length of arm of the thrust force, we can obtain the thrust of the thruster.

The physical picture of the thrust test bench is shown in Fig. 9. The thrust bench is a horizontal torsion pendulum. The electromagnetic standard force generator is composed of two parts: one is the permanent magnet installed on the torsion pendulum, and the other is the electromagnetic spiral coil installed on the multi-axis displacement bench. When a current is applied to the electromagnetic coil, an ampere force is generated between the electromagnetic coil and the permanent magnet, and the force is detected by a high-precision electronic balance. The electromagnetic standard force generator outputs a known electromagnetic standard force to drive the torsion pendulum to rotate. This known electromagnetic force, combined with the deflection displacement of the torsion pendulum, can give the torsion coefficient of the elastic element. In addition, a damper is also installed to make the torsion pendulum stable quickly and improve the anti-interference performance of the device.

Thrust Test Results

After the vacuum degree reaches 50 Pa, the air pressure at the nozzle inlet is manually adjusted to increase from 50 to 500 kPa in steps of 50 kPa. The corresponding thrust at each step of air pressure is shown in Fig. 10.

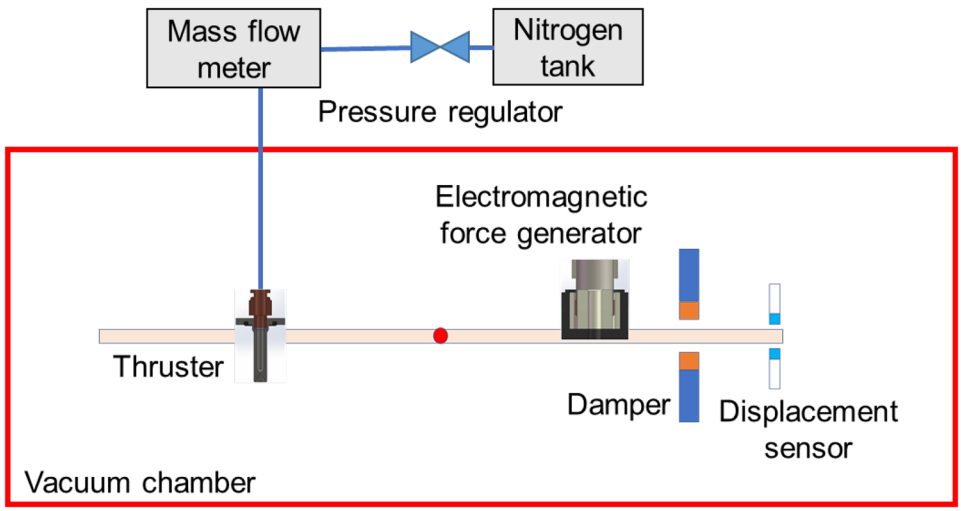

Fig. 8 Layout of thrust measurement experiment

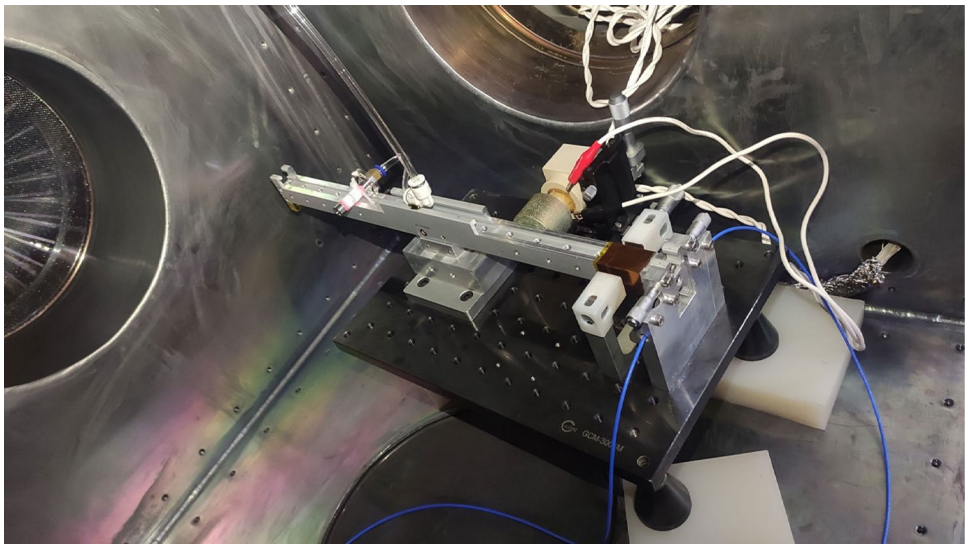

Fig. 9 Thrust measuring bench

Figure 11 is obtained by extracting air pressure data and corresponding thrust data for the first-order fitting. The fitting equation is:

$$F = 0.2517 * p - 1.0423 \tag{9}$$

The linear correlation coefficient is 0.9999. It can be seen that the thrust is proportional to the air pressure. This also proves the correctness of the scheme of obtaining the corresponding thrust by adjusting the pressure of the air path, which can meet the requirements of 50mN and 100mN of thrust. The maximum thrust is about 130mN, leaving a margin for the desired values of thrust.

Accelerometer Calibration

The microgravity level is one of the key technical indicators of drop tower, and it is also an important influencing factor on various experiments conducted in the drop tower. Precise measurement of the microgravity level of drop tower is essential to its construction and operation. According to the above, the microgravity level of drop tower is mostly between 10^{-2}g and 10^{-6}g. For the single capsule structure, the residual acceleration of the capsule is mainly caused by the aerodynamic resistance acting on the capsule. For the double capsule structure, the residual acceleration of the inner capsule is mainly caused by the frictional resistance acting on it by the gas between inner and outer capsules and the vibration of the inner capsule. The microgravity level of drop tower is directly measured by the high-precision accelerometer.

The measurement system adopts the JHT-I-H-3 three-axis accelerometer by Shaanxi Aerospace Great Wall Co., Ltd.. The sampling rate is 100 Hz, and the accelerometer has its own temperature compensation. Technical parameters of the accelerometer are shown in Table 2.

In order to accurately measure the falling acceleration, the accelerometer is calibrated on the single axis turntable with a resolution of 0.01'' at Beijing Institute of Aerospace Control Devices. As shown in Fig. 12, the single axis turntable rotates around the Y axis and uses the four-position tumbling method to calibrate the X and Z axes of the accelerometer.

The expression of acceleration output is

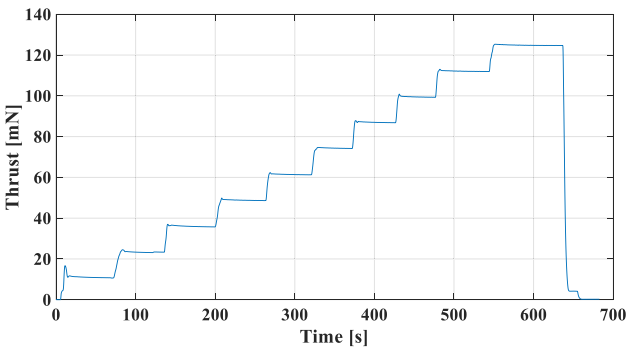

Fig. 10 Thrust measurement results

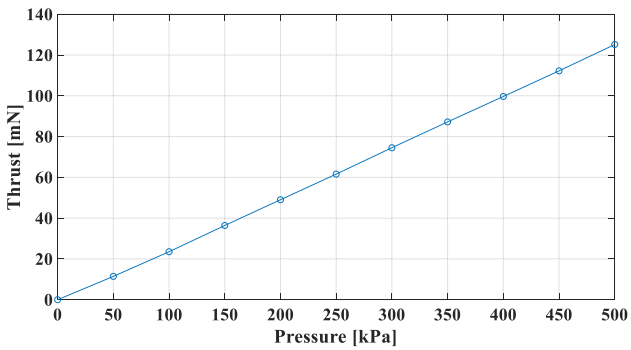

Fig. 11 Relationship between thrust and air pressure

Table 2 Technical indexes and parameters of accelerometer

No.	Parameter name	unit	Parameter index
1	Bias	mg	<3
2	Scaling factor	mA/g	1.2 ± 0.2
3	Second order nonlinearity	ug/g^2	<10
4	Bias temperature coefficient	ug/C	<20
5	Scaling factor temperature coefficient	ppm/C	<20
6	Bias stability	ug	<20
7	Scaling factor stability	ppm	<20
8	Second order nonlinearity stability	ug/g^2	<10
9	Natural frequency	Hz	800
10	Range	g	± 2
11	Resolution	g	1×10^{-6}

$$a_{out} = K_1\left(K_0 + a + K_2 a^2\right) \tag{10}$$

where

a_{out} Accelerometer output

K_1 Scaling factor

K_0 bias

K_2 Second order nonlinearity

a real acceleration

As in reference (Luo et al. 2021), the second-order nonlinear term can be neglected, and the scale factor K_1 and bias K_0 of the X axis of the accelerometer can be obtained according to the four-position method. As shown in Fig. 13, the X-axis scale factor is $\overline{K_1}$= 1.000677, and the standard deviation of K_1 is σ_{K_1}= 3.5e-05; the X-axis bias is $\overline{K_0}$ =-4.4630e-04g, and the standard deviation of K_0 is σ_{K_0}= 1.1964e-05g. Therefore, the measurement accuracy of the accelerometer is better than 15ug, which can meet the measurement requirements.

System Construction and Experiment

System Construction

The experimental system consists of four layers in total. As shown in Fig. 14, the first layer is the electric control box of the inner capsule, the second layer contains the accelerometer and the data acquisition system, the third layer is the pressure control system of cold-gas micro thrusters, and the fourth layer is equipped with micro thrusters that are distributed as shown in Fig. 15. There are a total of 24 micro thrusters, of which the thrusters of No. 4, No. 6, No. 19 and No. 20 have a thrust of 50mN, and the other thrusters have a thrust of 100mN.

Two accelerometers are installed on the second layer of the inner capsule. Accelerometer 1 monitors the microgravity level during the falling process with a range of ± 2g, and accelerometer 2 monitors the impact acceleration during the falling process with a range of ± 50g, as shown in the left figure of Fig. 16. The infrared laser

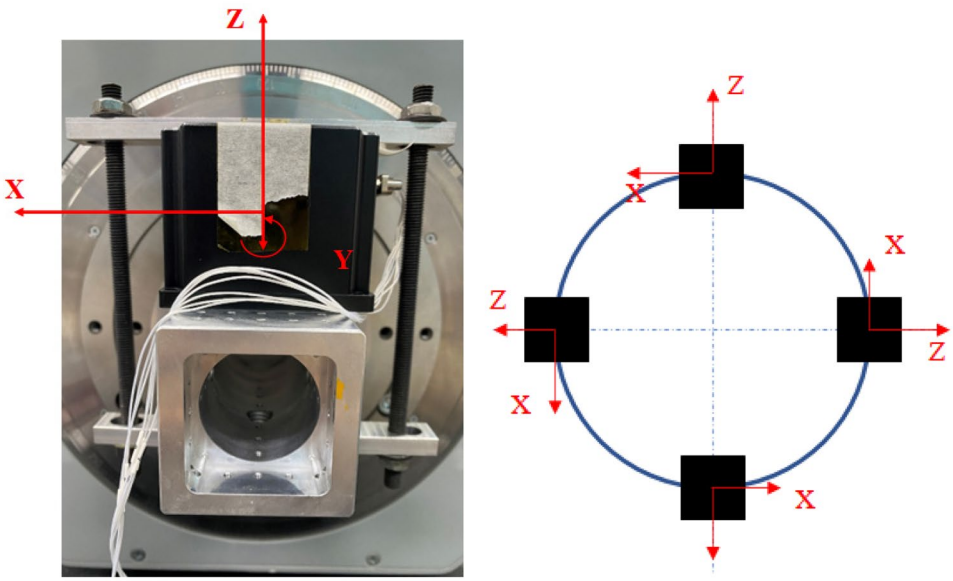

Fig. 12 Single axis turntable and four-position tumbling method

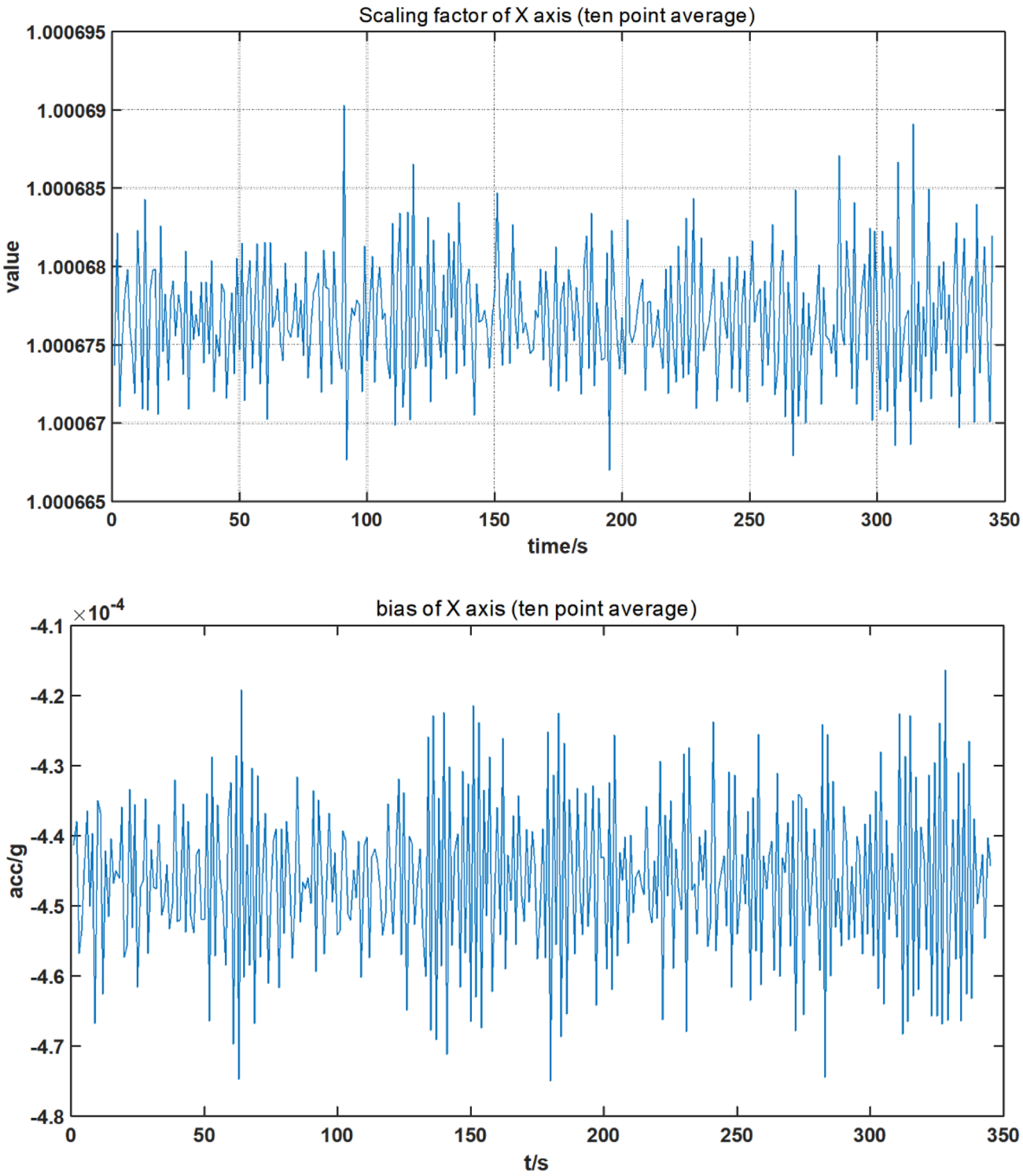

Fig. 13 Scale factor K1 and bias K0 of accelerometer

displacement sensors are installed outside the upper shell of the inner capsule to measure the distance between the

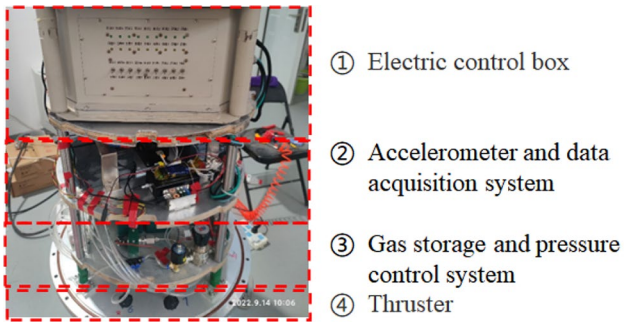

Fig. 14 Inner capsule experimental platform

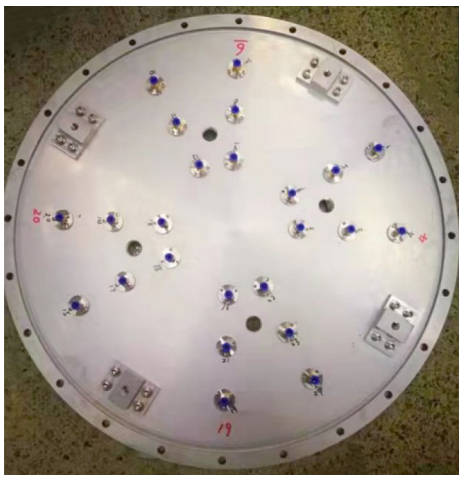

Fig. 15 Installation diagram of micro thrusters

inner capsule and the outer capsule during the free fall, as shown in the right figure of Fig. 16.

Experimental Process

According to the project objectives, there are three working modes of capsule falling: the first is the double capsule free falling mode, which offers a 10^{-5}g experimental environment; in the second mode, four 50mN micro thrusters in the inner capsule are activated 0.5s before the capsule starts to fall, and they are turned off at 2s after the falling starts, in order to achieve a 10^{-4}g microgravity level; in the third mode, 20 100mN micro thrusters in the inner capsule are turned on 0.5s before the capsule starts to fall, and they are turned off at 2.5s after the falling starts, in order to achieve a 10^{-3}g microgravity level, as shown in Fig. 17.

Results and Analysis

According to the experimental process, 16 double capsule mode experiments are carried out, the experimental data of residual acceleration of the inner capsule under different working conditions are obtained, and the correctness of the scheme of microgravity level control is verified. To analyze the sources of residual acceleration of the inner and outer capsules, models for residual acceleration analysis are established for the inner and outer capsules. Theoretical analysis and numerical simulation are performed to calculate the residual acceleration of the inner and outer capsule, and spectral analysis is used to analyze the sources of micro vibration of the inner capsule.

Experimental Results

The entire acceleration process of the free fall is 3.6 s, including the release process of 0.2 s, as shown in Fig. 18. The whole recovery process lasts about 15 s, with a maximum overload of about 14g, and the capsule finally falls into a stable 1g state. During the process of falling, the

Fig. 16 Accelerometers and infrared laser displacement sensors

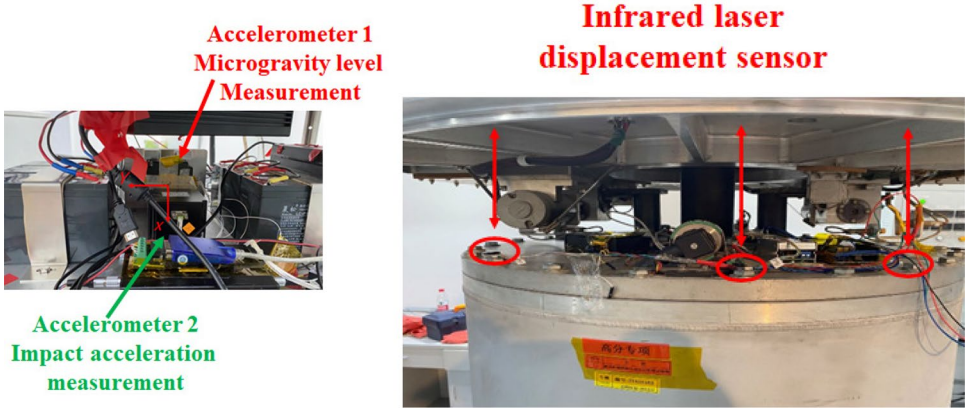

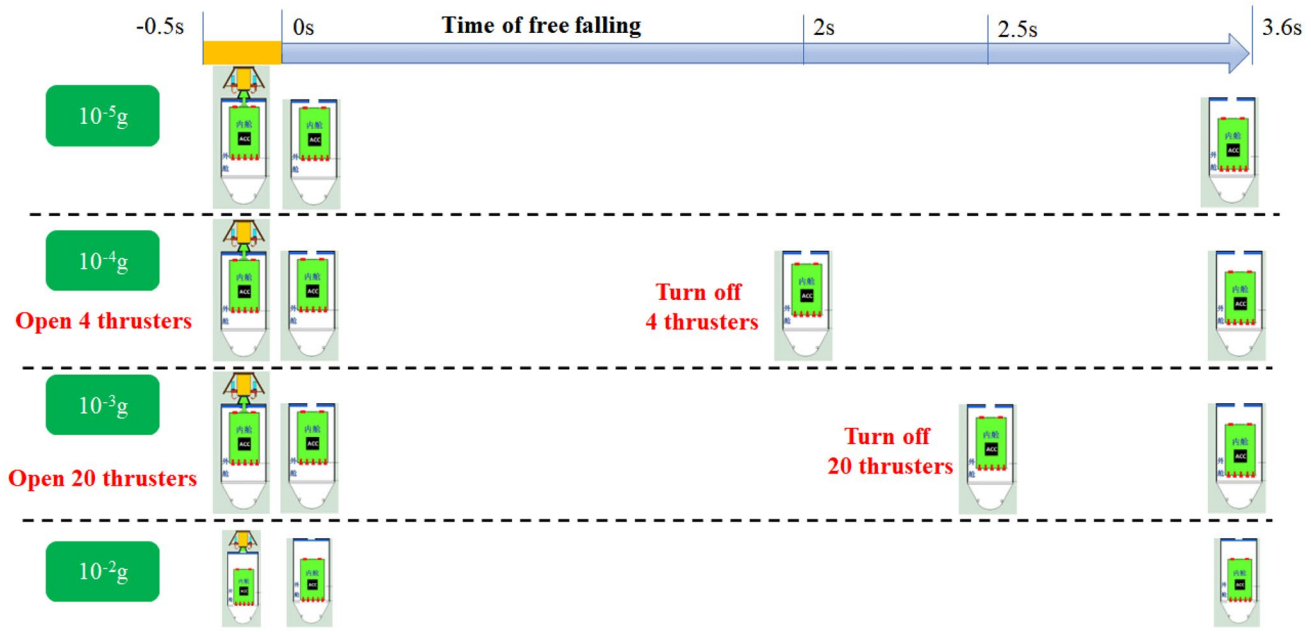

Fig. 17 Experimental process

accelerations of the capsule in both non-falling directions are less than 3g, as shown in Fig. 19.

The results of the 10^{-5}g microgravity experiment are described as below. According to the experimental process design, in this experiment, both capsules fall freely. The microgravity level of the inner capsule in the process of free fall is shown in Fig. 20. The residue acceleration of the capsule at 1.5s after the falling starts reaches [10^{-4}, 10^{-5}] g, which is 10^{-5}g microgravity level. To confirm this result, we compare it with the test results in reference (Min et al. 2021). In 2019, Lanzhou Institute of Technology and Physics carried out an electrostatic accelerometer test in Beijing drop tower. In the last 0.5s of the falling, the residue acceleration of the inner capsule reached 58ug in the falling direction, and reached 13ug in the non-falling directions. The results are similar to those measured in this experiment. In our experiment, in the last 0.5s of the falling process, the residue acceleration has reached 60ug, as shown in Fig. 21. This result is significantly smaller than the result of 2×10^{-4}g in the falling direction in reference (Liu et al. 2016).

Figure 22 shows the results of 10^{-4}g microgravity experiment. In this experiment, four 50mN thrusters are activated 0.5s before the release of capsules, and the cold-gas micro thrusters are turned off at about 2.5s after the

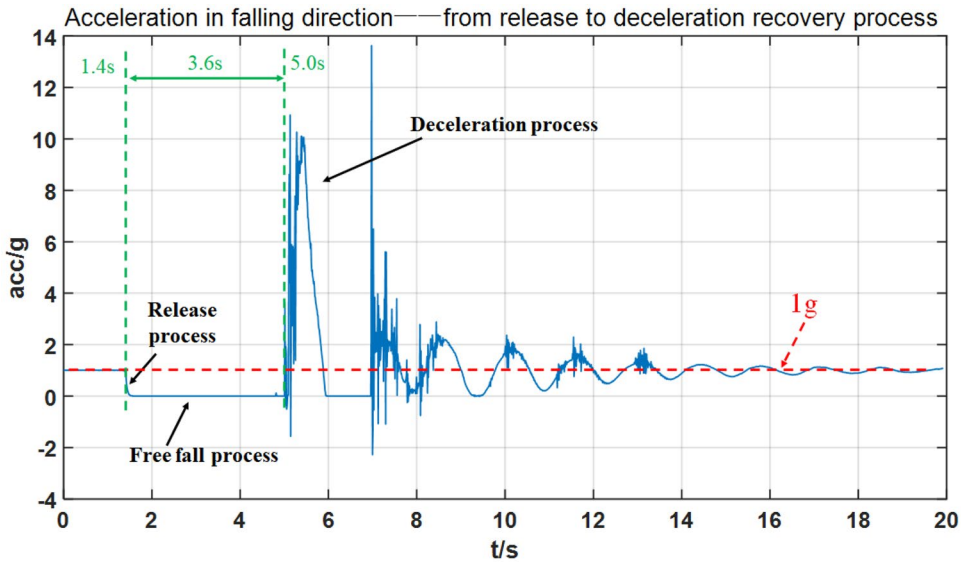

Fig. 18 Acceleration of inner capsule in the falling direction

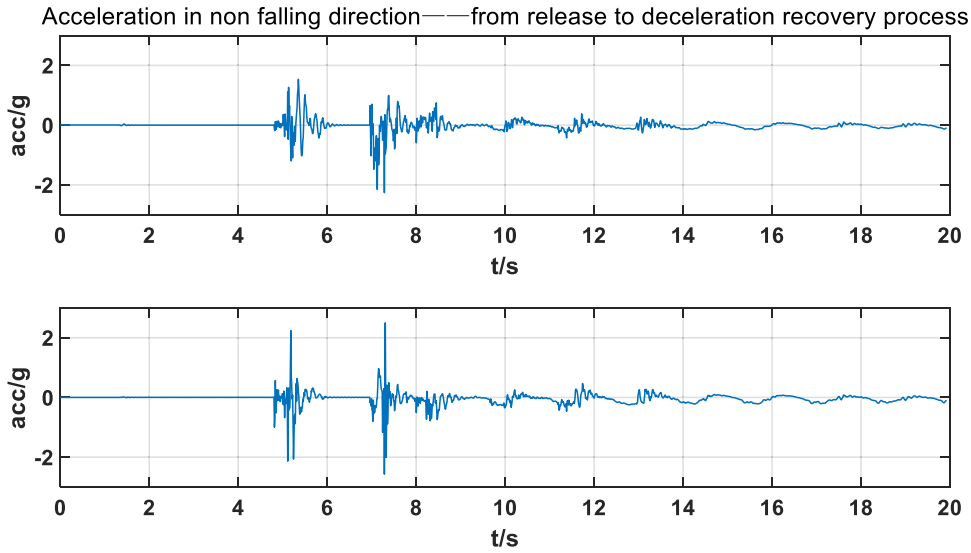

Fig. 19 Accelerations of inner capsule in non-falling directions

release. It can be seen from Fig. 22 that starting from 0.3 s, the residue acceleration of the capsule reaches [10^{-3},10^{-4}] g, meeting the design target. At 2.5 s, the vibration caused by turning off the thrusters can be observed.

Figure 23 shows the results of 10^{-3}g microgravity experiment. In this experiment, 20 100mN thrusters are activated 0.5s before the release of capsules, and the cold-gas micro thrusters are turned off at about 2.5s after the release. It can be seen from Fig. 23 that starting from 0.5 s, the residue acceleration of the capsule reaches [10^{-2},10^{-3}] g, meeting the design target. At 2.5 s, the capsule falls into the 10^{-4}g state. At 3 s, the vibration caused by turning off the thrusters is observed.

Result Analysis

Theoretical Analysis and Numerical Simulation of Residual Acceleration of the Outer Capsule

The outer capsule freely falls in the atmospheric environment and is mainly affected by atmospheric resistance. Theoretical analysis and CFD numerical simulation methods are used to calculate the residual acceleration of the outer capsule during the falling process. The dynamic equations of motion of the outer capsule in the falling process are

$$m_0 \frac{dv_0}{dt} = m_0 g_0 - F_z \tag{11}$$

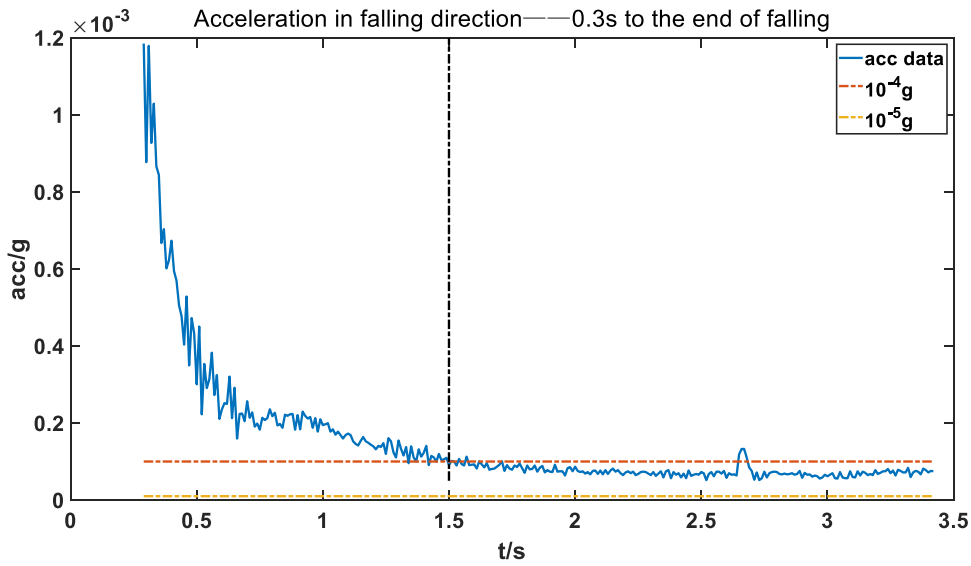

Fig. 20 Microgravity level of inner capsule during free fall

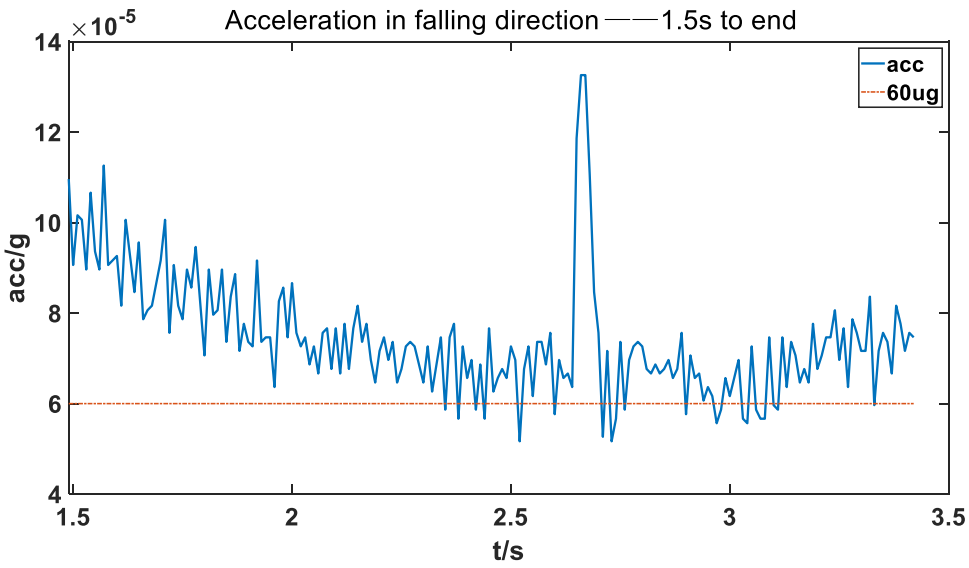

Fig. 21 Residual acceleration of inner capsule at 1.5s after the falling starts

$$F_z = \frac{1}{2} C_d \rho_0 S_0 v_0^2 \tag{12}$$

In these equations, the mass of the outer capsule $m_0 = 400$ kg, the gravitational acceleration $g_0 = 9.8015$ m/s^2, the atmospheric density $\rho_0 = 1.293$ kg/m^3, the resistance coefficient C_d, and the cross-sectional area of the outer capsule $S_0 = 0.8$ m^2. The relationship between residual acceleration of the outer capsule a_z and duration of microgravity t is as follows (Xia 1995)

$$a_z = g_0 \frac{e^{\beta t} - 1}{e^{\beta t} + 1} \tag{13}$$

$$\beta = \sqrt{2 C_d \rho_0 S_0 g_0 / m_0} \tag{14}$$

Assuming that the resistance coefficient of the outer capsule is constant throughout the entire process of free falling, and the initial velocity of the capsule $v_0(t_0) = 0$.

$$a_{z0} = g_0 tanh^2 \sqrt{\frac{C_d \rho_0 S_0 g_0}{2 m_0}} t \tag{15}$$

To accurately analyze the residual acceleration of the outer capsule during the free fall, the Ansys-Fluent software is used to calculate the resistance. Figure 24 shows the calculation model and foreground grid. The k- ϵ turbulence model and the standard wall function (SWF) are selected for the calculation. The gravitational acceleration along the Z-axis direction is g_0, and a dynamic grid model is selected.

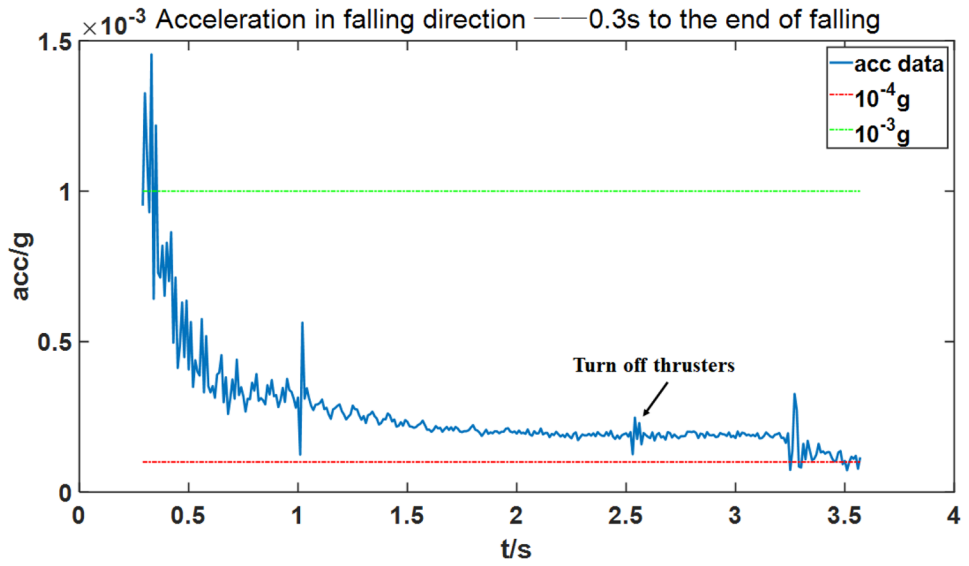

Fig. 22 10^{-4}g microgravity experiment

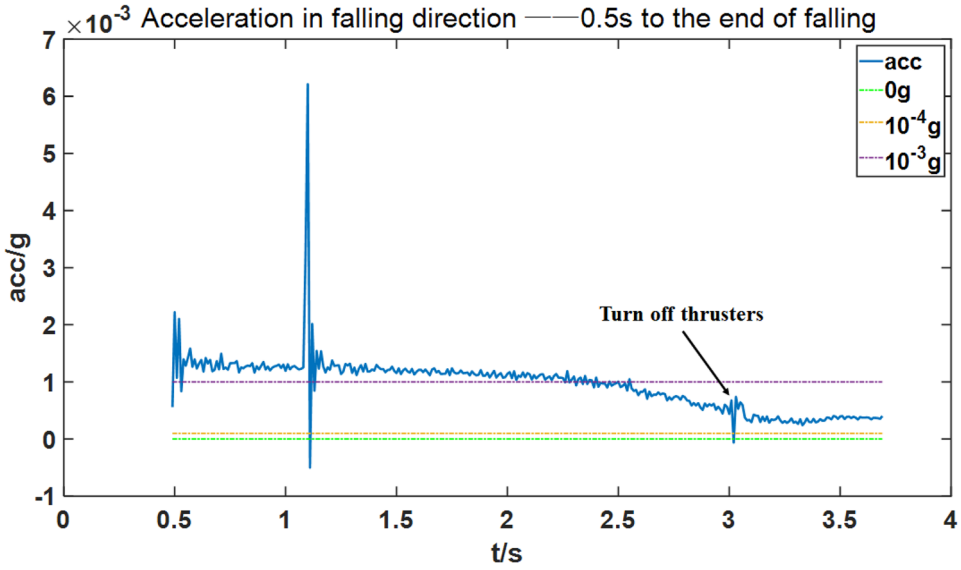

Fig. 23 10^{-3}g microgravity experiment

The results of theoretical analysis and CFD simulation are shown in Fig. 25. According to Eq. (15), the residual accelerations of the outer capsule are calculated with the drag coefficient Cd = 0.2, 0.3, 0.4, and 0.5 respectively. When Cd = 0.3, the theoretical calculation value of the residual acceleration of the outer capsule is relatively close to the value from the CFD simulation. According to the results of theoretical analysis and calculation, when Cd = 0.3, at the end of the falling, t = 3.5 s, and $a_{z0} = 0.045g$. The CFD calculation results show that the residual acceleration of the outer capsule at the end of the falling is 0.042g. The CFD simulation results show oscillations during 2 to 3.5 s. The main source of the resistance acting on the outer capsule is the pressure difference between the top and bottom of the outer capsule. At the end of the falling, the detachment of the vortex street at the rear of the outer capsule causes pressure pulsations at the rear, leading to pressure oscillations, which is not predicted by the theoretical analysis.

An infrared laser displacement sensor is installed on the top of the inner capsule to record the displacement between the inner and outer capsules during the free fall. The displacement difference is mainly caused by the residual acceleration of the outer capsule. The infrared laser displacement sensor records displacement changes and calculates displacement values under different values of resistance coefficient, Cd, as shown in Fig. 26. When Cd = 0.4, the theoretical calculation value of the displacement difference is close to the value obtained from the CFD simulation, which is 0.61m. However, both displacement values are smaller than the actual measurement value. When Cd = 0.5, the calculated displacement difference is 0.76m, which is close to the recorded value. From the trend

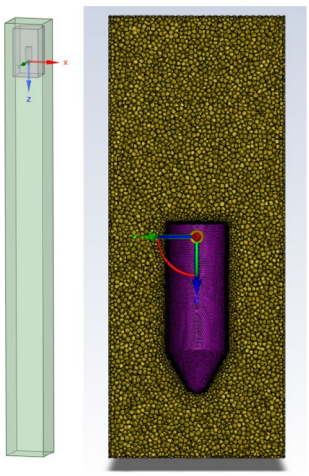

Fig. 24 the calculation model and foreground grid

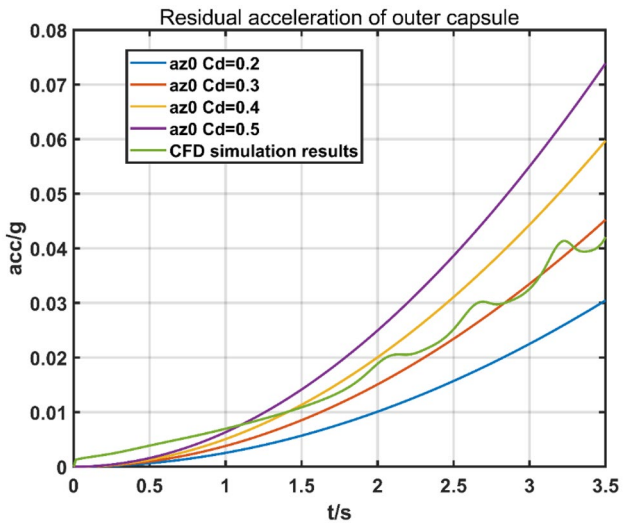

Fig. 25 Residual acceleration of outer capsule with different Cd values. Compared with CFD calculation results

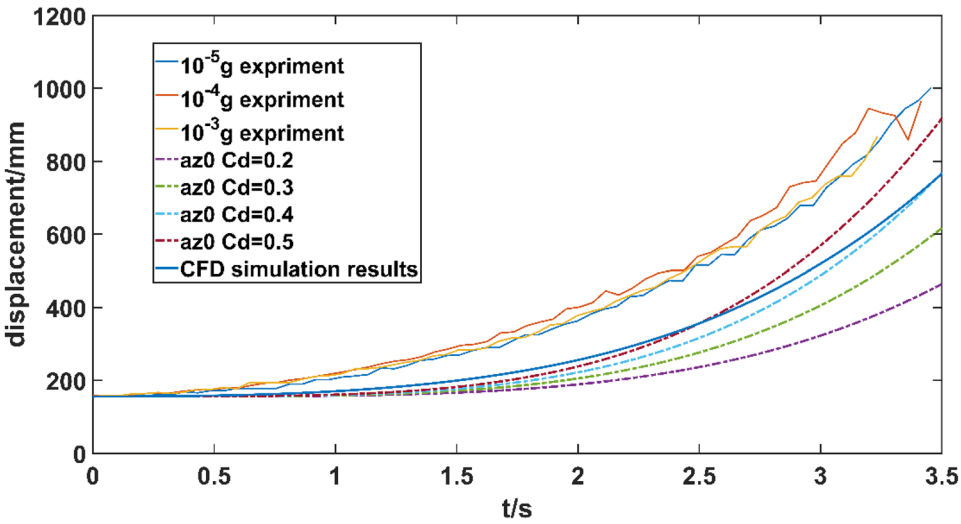

Fig. 26 Calculated and experimental values of relative displacement between inner and outer capsules

of the curves, we can see that in the range between 0.5s and 3 s, the theoretical calculation values are significantly smaller than the actual measurement values, indicating that the modeling resistance used in Eq. (12) is relatively small.

Theoretical Analysis and Numerical Simulation of Residual Acceleration of the Inner Capsule

In the double capsule operation mode, the inner capsule freely falls in an approximate vacuum environment inside the outer capsule. When the thrusters do not work, the air pressure between the inner and outer capsules is about $P_1 = 300$pa, and the gas density is ρ_1. The volume between the inner and outer capsules is $V_1 = 1.4876\text{m}^3$. According to the state equation of ideal gas,

$$\rho_1 = \frac{P_1}{P_0}\rho_0 \tag{16}$$

where P_0 is atmospheric pressure under standard state. $\rho_1 = 3.9\ \text{kg} \times 10^{-3}/\text{m}^3$, In the initial state, the mean free path of air molecules

$$\overline{\lambda} = \frac{kT}{\sqrt{2}\pi d^2 P_1} \tag{17}$$

where, d is the effective diameter of air molecules, and T is the temperature. According to Eq. (17) the mean free path of air molecules corresponds to the pressure of 6.7×10^{-5}m. The Knudsen number is less than 0.1 and the air flows continuously. Therefore, a continuous medium model can be used to calculate the resistance acting on the inner capsule.

$$F_D = \frac{1}{2}C_D\rho_1 S_1 \left(v_1 - v_0\right)^2 \tag{18}$$

where, C_D is the resistance coefficient, S_1 is the cross-sectional area of the inner capsule, and v_1 is the velocity of the inner capsule. The dynamic equation of motion of the inner capsule is

$$m_1 \frac{dv_1}{dt} = m_1 g_0 - F_D \tag{19}$$

The numerical integration method is used to calculate the residual acceleration of the capsule during the falling

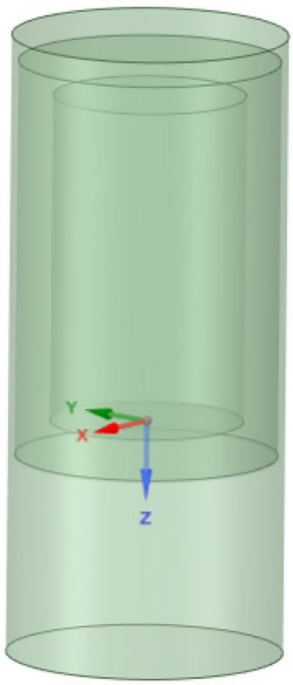

Fig. 27 Calculation model for residual acceleration of inner capsule

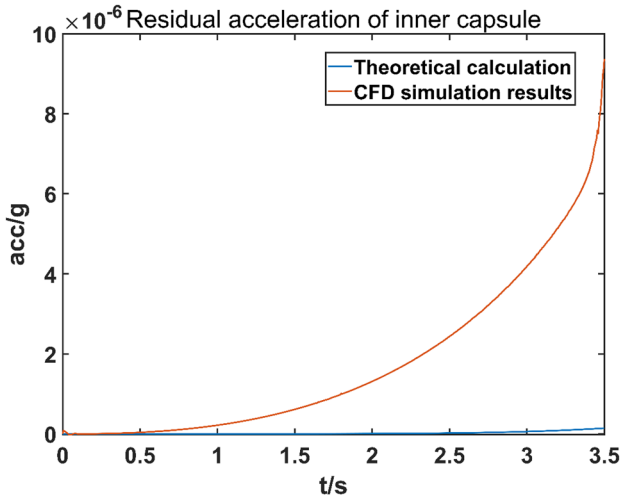

Fig. 28 Numerical integration and CFD calculation results

process. When the resistance coefficient of the outer capsule $Cd = 0.5$, the difference between the velocity of the outer capsule and that in the outer capsule absolute free fall is taken as the relative velocity between the inner and outer capsules.

$$\Delta v = gt - \sqrt{\frac{2m_0 g_0}{C_d \rho S}} tanh\left(\sqrt{\frac{C_d \rho_0 S_0 g_0}{2m}} t\right) \tag{20}$$

In order to model the falling process of the inner capsule more accurately, the ANSYS Fluent is used to calculate the residual acceleration of the inner capsule during the falling process. Figure 27 shows the calculation model, which uses a dynamic grid to simulate the falling process. The relative velocity between the inner and outer compartments is calculated using Eq. (20). The numerical integration and CFD calculation results are shown in Fig. 28.

From Fig. 28, the calculated value of the free falling residual acceleration from the CFD simulation is significantly greater than the calculated value from the theoretical analysis. At the end of the falling process, when $t = 3.5$ s, the residual acceleration from the CFD calculation reaches 10ug, and the value from the theoretical calculation is 0.15ug. Compared with actual measurements, the result of CFD calculation is significantly closer to the actual value, which indicates that using Eq. (18) to model the resistance of the inner capsule is inaccurate.

Analysis of Micro Vibrations of Inner Capsule

From the data measured by the accelerometer, there are micro vibrations of the inner capsule during the falling process of the $10^{-5} \sim 10^{-3}$g experiments. To analyze its source, a knocking experiment is conducted on the inner capsule before the start of the double capsule experiment, and the acceleration caused by the knocking is recorded by the accelerometer. Spectrum analysis is performed on the data of residual acceleration collected during the free-fall process of the double capsule experiment, and the acceleration is also recorded during the impact experiment, as shown in Fig. 29. A vibration with a frequency of approximately 43 Hz is recorded in both of the impact experiment and the free-fall process. So it is caused by the mode of the inner capsule itself.

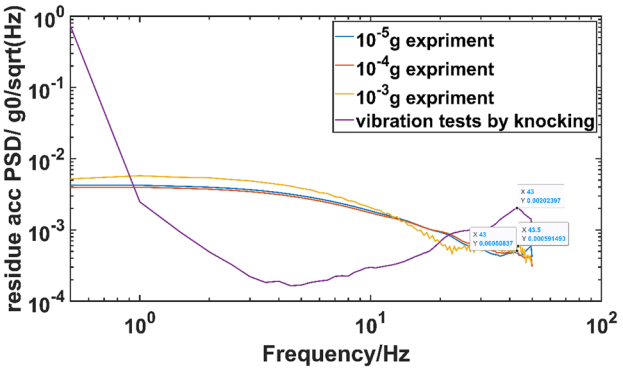

Fig. 29 spectrum diagram of micro vibrations of inner capsule

Conclusion

In this paper, the current status of Beijing drop tower is introduced in detail, and according to the requirements of the current scientific research on the equipment update in the drop tower, a scheme of the inner capsule cold-gas micro thruster deceleration control system based on the double capsule operation mode is proposed. A cold-gas micro thrust system is developed and the performance of the micro thrusters is measured. The accelerometer of the experiment are calibrated, and it is proved that the accelerometer can accurately measure the 10^{-5}g acceleration. The experimental scheme of 10^{-3}g ~ 10^{-5}g microgravity level control in the inner capsule is designed, and experiments are carried out according to the experimental scheme. The results show that the microgravity level in the inner capsule can reach 10^{-5}g in the free-falling state, and the falling acceleration of the inner capsule can be adjusted between $10^{-3} \sim 10^{-5}$g in the control state. Theoretical analysis and numerical simulation are performed to calculate the residual acceleration of the inner and outer capsule, and spectral analysis is used to analyze the sources of micro vibration of the inner capsule. The results show that the residual acceleration calculated by CFD numerical simulation and the difference in displacement between the inner

and outer capsules are closer to the actual measured values, and the residual acceleration of the inner and outer capsules mainly comes from aerodynamic pressure resistance. During the free-falling process of the inner capsule, the initial residual acceleration mainly comes from the vibration of the inner capsule itself excited by the release process.

Acknowledgements We appreciated Prof. Jianfu Zhao from Institute of Mechanics, Chinese Academy of Sciences for offering valuable suggestions.

Authors' Contributions All authors have contributed to the study of concepts and design. Chu Zhang and Chao Yang wrote the manuscript. Liang Hu and Yifan Zhao completed the experiment and collected data. Shuyang Chen completed CFD simulation. Li Duan and Qi Kang offered guidance and support.

Funding This research was funded by National key R&D plan (No. 2021YFC2202604) and the National Natural Science Foundation of China (No. 12032020). Thanks for the support of China Manned Space Station Engineering Program (2018-254).

Availability of Data and Material The data of this article can be obtained by contacting the corresponding author.

Declarations

Ethics Approval Not applicable.

Consent to Participate Not applicable.

Consent for Publication Not applicable.

Conflicts of Interest The authors declare no competing financial interest.

References

Chen, S., Duan, L., Kang, Q.: Study on propellant management device in plate surface tension tanks. Acta. Mech. Sin. **37**(10), 12 (2021)

Glenn Research Center.: NASA: Zero gravity research facility user's guide (2017)

Gu Y.: The China Space Station: a new opportunity for space science. Nat. Sci. Rev. (2021)

Hu, Q., Chen, J., Li, Y.: Numerical simulation for reorientation of prototype in a van tank under microgravity. Aerospace Control and Application **35**(6), 4 (2009)

Koide, A.: Drop-shaft type microgravity facility accommodating 10-seconds microgravity. J. Japan Soc. Microg. Appl. **18**(3), 136–139 (2001)

Liu, T.Y., Wu, Q.P., Sun, B.Q., et al.: Microgravity Level Measurement of the Beijing Drop Tower Using a Sensitive Accelerometer. Rep **6**(1), 31632 (2016)

Luo, L., Zhou, H., Sun, Y., et al.: Tsinghua University Freefall Facility (TUFF): A 2.2 Second Drop Tunnel for Microgravity Research. Microgravity Sci. Technol. **33**(2), 26 (2021)

Min, J., Wang, Z.L., Li, Y.P., et al.: Drop tower tests of Taiji-1 inertial sensor substitute. npj Microgravity **7**, 25 (2021). https://doi.org/10.1038/s41526-021-00154-8

Nikhil, V.V., Abhilash, N., Niketh, P., et al.: The 2.5 s Microgravity Drop Tower at National Centre for Combustion Research and Development (NCCRD), Indian Institute of Technology Madras. Microgravity Sci. Technol. **30**, 663–673 (2018)

Peng, Y.Q., Zhang, L.B., Cai, Z.G., et al.: Overview of the Mars climate station for Tianwen-1 mission. Earth Planet Phys. (4), (2020)

Raj, R., Kim, J., Mcquillen, J.: Gravity Scaling Parameter for Pool Boiling Heat Transfer. J. Heat Transf. **132** (9), 1187–1191 (2010)

Selig, H., Dittus, H., LaMmerzahl, C.: Drop Tower Microgravity Improvement Towards the Nano-g Level for the MICROSCOPE Payload Tests. Microgravity Sci. Technol. **22**(4), 539–549 (2010)

Steinberg, T.: Reduced gravity testing and research capabilities at Queensland University of Technology's New 2.0 Second Drop Tower. Adv. Mater. Res. **32**, 21–24 (2008)

Wang, C.X., Xu, S.H., Sun, Z.W., et al.: A study of the influence of initial liquid volume on the capillary flow in an interior corner under microgravity. Int. J. Heat Mass Transf. **53**(9–10), 1801–1807 (2010)

Xia, Y.: Microgravity drop tower test technology and its application (I). Struct. Environ. **38**, 22–31 (1995)

Yang, W., Zhang, Y., Liu, B., et al.: Volatile Ejection in Jet Manner and its Influence on Combustion of Isolated Coal Particles. Microgravity Sci. Technol. **34**(5), 1–9 (2022)

Yang, Y.J., Chen, X.Q., Huang, Y.Y., et al.: Experimental study on pool boiling of distilled water and HFE7500 fluid under microgravity - ScienceDirect. Acta Astronaut. **143**, 362–371 (2018)

Yidong, G.U., Ming, G.A., et al.: Space Research Plan of China's Space Station. Chinese J. Space Sci. (5), 5 (2016)

Zhang, J., Dong, W., Wang, Z., et al.: Development of a New Microgravity Experiment Facility with Electromagnetic Launch. Microgravity Sci. Technol. **33**, 68 (2021)

Zhang, X., Yuan, L., Wu, W., Tian, L., Yao, K.: Some key technics of drop tower experiment device of National Microgravity Laboratory (China) (NMLC). Sci. China Technol. Sci. (2005)

Zhao, J., Du, W.: Gravity scaling law of heat transfer in nucleate pool boiling. Chinese J. **65**(17), 1629–1637 (2020)

Zhou, C., Tang, H., Li, X., et al.: Chang'E-5 samples reveal high water content in lunar minerals. Nat. Commun. **13**, 5336 (2022)

Zhu, Z.Q., Brutin, D., Liu, Q.S., Wang, Y., Mourembles, A., Xie, J.C., Tadrist, L.: Experimental Investigation of Pendant and Sessile Drops in Microgravity. Microgravity Sci. Technol. (2010)